

Accepted Manuscript

Title: Visual and in situ Raman spectroscopic observations of the liquid-liquid immiscibility in aqueous uranyl sulfate solutions at temperatures up to 420 °C

Author: Xiaolin Wang Ye Wan Wexuan Hu I-Ming Chou
Shenyang Cai Nan Lin Qiang Zhu Zhen Li



PII: S0896-8446(16)30042-0

DOI: <http://dx.doi.org/doi:10.1016/j.supflu.2016.03.005>

Reference: SUPFLU 3583

To appear in: *J. of Supercritical Fluids*

Received date: 30-12-2015

Revised date: 2-3-2016

Accepted date: 7-3-2016

Please cite this article as: Xiaolin Wang, Ye Wan, Wexuan Hu, I-Ming Chou, Shenyang Cai, Nan Lin, Qiang Zhu, Zhen Li, Visual and in situ Raman spectroscopic observations of the liquid-liquid immiscibility in aqueous uranyl sulfate solutions at temperatures up to 420^{circ}C, The Journal of Supercritical Fluids <http://dx.doi.org/10.1016/j.supflu.2016.03.005>

This is a PDF file of an unedited manuscript that has been accepted for publication. As a service to our customers we are providing this early version of the manuscript. The manuscript will undergo copyediting, typesetting, and review of the resulting proof before it is published in its final form. Please note that during the production process errors may be discovered which could affect the content, and all legal disclaimers that apply to the journal pertain.

Visual and in situ Raman spectroscopic observations of the liquid-liquid immiscibility in aqueous uranyl sulfate solutions at temperatures up to 420 °C

Xiaolin Wang ^{a, b}, Ye Wan ^a, Wenzuan Hu ^{a, b}, I-Ming Chou ^c, Shenyang Cai ^a, Nan Lin ^a, Qiang Zhu ^a and Zhen Li ^d

^a State Key Laboratory for Mineral Deposits Research, School of Earth Sciences and Engineering, Nanjing University, Nanjing, Jiangsu 210023, China

^b Institute of Energy Sciences, Nanjing University, Nanjing, Jiangsu 210023, China

^c Laboratory for Experimental Study Under Deep-sea Extreme Conditions, Sanya Institute of Deep-sea Science and Engineering, Chinese Academy of Sciences, Sanya, Hainan 572000, China

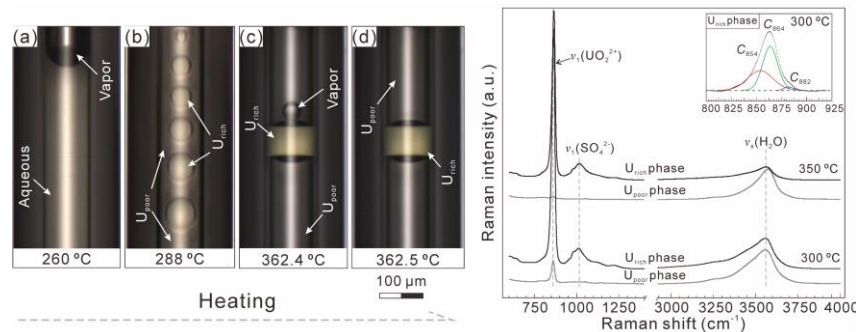
^d Department of Applied Geology, Curtin University, Perth, WA 6845, Australia

Corresponding author: Xiaolin Wang

Department of Earth Sciences
Nanjing University
163 Xianlin Ave.
Nanjing
Jiangsu 210023
P.R. China

Tel: +86 (25) 89680867
Fax: +86 (25) 89680867
Email: xlinwang@nju.edu.cn (X. Wang)

Graphical abstract



Highlights

1. Liquid-liquid immiscibility was observed in aqueous UO_2SO_4 solution at $\geq 285.8 \pm 0.5$ °C.
2. The immiscible liquids are either UO_2SO_4 -rich (U_{rich}) or UO_2SO_4 -poor (U_{poor}).
3. Analyses of UO_2^{2+} and SO_4^{2-} spectra imply increasing ion association upon heating.
4. Decrease of ion hydration in U_{rich} phase due to increasing concentration upon heating.
5. Reversible strong UO_2^{2+} – SO_4^{2-} association results in the liquid-liquid immiscibility.

Abstract

The phase behaviors of aqueous UO_2SO_4 solutions were investigated in situ with a microscope and a Raman spectrometer at temperatures from 25 to 420 °C. Results show that aqueous UO_2SO_4 solution separated into UO_2SO_4 -rich (U_{rich}) and UO_2SO_4 -poor (U_{poor}) liquid phases coexisted with a vapor phase at $\geq 285.8 \pm 0.5$ °C. Both visual and Raman spectroscopic investigations suggest that a reversible strong UO_2^{2+} – SO_4^{2-} association was responsible for the liquid-liquid immiscibility in aqueous UO_2SO_4 solutions. Main evidences were summarized as: (1) the liquid-liquid phase separation temperature decreases with increasing UO_2SO_4 concentration up to 0.54 mol/kg, and then increased at greater concentrations, characterizing a lower critical solution temperature (LCST) at 285.8 °C±0.5 °C. LCST is commonly accepted as a diagnostic feature of polymer solutions; (2) analyses of the shapes of the Raman spectra of $\nu_1(\text{UO}_2^{2+})$ and $\nu_1(\text{SO}_4^{2-})$ bands show that the UO_2^{2+} – SO_4^{2-} association becomes stronger at elevated temperatures, especially in the immiscible U_{rich} phase;

and (3) with increasing temperature, the U_{rich} phase becomes more concentrated, whereas the U_{poor} phase becomes more dilute, indicating that the hydration of UO_2^{2+} and SO_4^{2-} cannot be maintained in the U_{rich} phase. Destruction of the hydration spheres of UO_2^{2+} and SO_4^{2-} further favors the ion association in the U_{rich} phase. These results are important for describing similar sulfate solutions at elevated temperatures, especially under supercritical conditions.

Key words: $\text{UO}_2\text{SO}_4\text{-H}_2\text{O}$; liquid-liquid immiscibility; Raman spectroscopy; ion association.

1. Introduction

It has been shown that the density, viscosity, dielectric constant and ion product of pure water are significantly reduced at elevated temperatures, especially in supercritical water (SCW) [1–2]. Owing to these remarkably changes, SCW has wide industrial applications. For example, it has been considered as an important medium for the disposal of waste organic compounds [2]. In general, SCW is found to be miscible with many organic compounds and gases, but shows negligible solubilities of salts. Previous studies confirmed that the solubilities of many alkali metal sulfates were significantly decreased in SCW and sulfates precipitated from supercritical solutions [2–5]. However, many aqueous sulfate solutions were reported to show intriguing liquid-liquid immiscibility at elevated temperatures [6–7]; the homogeneous aqueous solution separated into two immiscible liquid phases coexisting with vapor phase. It should be noted that no precipitate was formed in this

case, even though the temperature reached the supercritical point of water. Among these sulfate–water systems, the UO_2SO_4 – H_2O system has been studied for a long time because the liquid–liquid phase separation temperature constitutes the upper limit for the operation of aqueous homogeneous reactors [8–12]. For example, Marshall and coworkers observed the liquid–liquid immiscibility at elevated temperatures and pressures (280–450 °C, 7.5–180 MPa) [12]. The compositions of the immiscible liquid phases were also analyzed using quenching method [10]. Although they postulated that the liquid–liquid immiscibility might be in close association with the polymerization between UO_2^{2+} and SO_4^{2-} [12], no detailed information on the ion interactions in the two immiscible liquid phases is available. In addition, disagreement exists among the reported lowest temperatures for the occurrence of the liquid–liquid immiscibility in aqueous UO_2SO_4 solutions. For instance, Secoy reported that the liquid–liquid immiscibility occurred at temperatures above 295.5 °C [8], whereas Marshall and Gill observed the critical liquid–liquid immiscibility temperature at 286 °C in 0.58–1.14 mol/kg UO_2SO_4 [12].

As to the association between UO_2^{2+} and SO_4^{2-} , Raman spectra of the $\nu_1(\text{UO}_2^{2+})$ band has been reported to be an effective indicator [13–16]; the coordination of UO_2^{2+} can increase the O=U=O length, causing the $\nu_1(\text{UO}_2^{2+})$ band shifts to lower wavenumber [13–14, 17–19]. In fact, Raman spectra of the $\nu_1(\text{SO}_4^{2-})$ band can also be used to investigate the ion interaction between UO_2^{2+} and SO_4^{2-} in aqueous solution because the complexation will influence the S-O vibrations of sulfate and cause a shift in the $\nu_1(\text{SO}_4^{2-})$ band, which has been well documented in aqueous MgSO_4 solutions

[20–24]. However, nearly all of the documented Raman spectroscopic descriptions of aqueous UO_2SO_4 solutions were conducted at ambient temperature and focused on the $v_1(\text{UO}_2^{2+})$ mode, which limits our knowledge on the $\text{UO}_2^{2+}\text{--SO}_4^{2-}$ association at high temperatures as well as the factors inducing the liquid-liquid immiscibility.

Here, fused silica capillary tube was used to construct the optical and spectroscopic cells containing UO_2SO_4 solutions. A Linkam CAP500 heating stage was used to control the sample temperature. Then, the liquid-liquid immiscibility was described *in situ* with microscope and Raman spectrometer. The main achievements include: (1) describing the high temperature liquid-liquid immiscibility in the $\text{UO}_2\text{SO}_4\text{--H}_2\text{O}$ system (≤ 420 °C) and measuring the temperatures for the occurrence of the liquid-liquid immiscibility at vapor saturated pressures (along a liquid-vapor curve); (2) documenting *in situ* Raman spectra of the $\text{UO}_2\text{SO}_4\text{--H}_2\text{O}$ system and investigating the $\text{UO}_2^{2+}\text{--SO}_4^{2-}$ interaction; and (3) investigating the variations of the UO_2SO_4 concentrations in the immiscible liquid phases by analyzing *in situ* Raman spectra.

2. Materials and methods

2.1. Optical cell preparation

Deionized water and guaranteed reagent $\text{UO}_2\text{SO}_4\cdot 2\text{H}_2\text{O}$ (99.9 mass %, Hubei Chushengwei Chemistry Co., Ltd.) were used to prepare aqueous uranyl sulfate solutions with the following molality: 0.18, 0.36, 0.54, 0.71, 0.88 and 1.04 mol/kg. Fused silica capillary tubes (Polymicro Technologies, LLC) with 300 μm outer diameter and 100 μm inner diameter were used to construct the optical and

spectroscopic cells (fused silica capillary capsule, FSCC). This type of optical cell was first introduced by Chou et al. [25], and the sample loading procedures were well described in previous literatures [24–25]. First, one end of the tube was sealed with a hydrogen-oxygen flame. Then, the aqueous solution was loaded into the tube and centrifuged to the sealed end. At last, the sealed end of the tube was inserted into water and the open end was sealed via fusion in a hydrogen-oxygen flame. Since samples were heated along a liquid-vapor curve, accurate pressures at the liquid-liquid phase separation points inside FSCCs were unknown and they varied with temperature and UO_2SO_4 concentration. Different from our previous studies, in order to avoid the reduction of UO_2^{2+} , the silica tube was not vacuumed before the sealing of the FSCC using hydrogen-oxygen flame [19]. The FSCC has enough mechanical resistance at high temperature (*ca.* 500–650 °C) and higher pressure (*ca.* 100~300 MPa), and has already been used as a reactor for subcritical and supercritical reactions, especially for those involving the hydrolysis of many organic waste compounds [26].

2.2. Microscopic observation and Raman characterization

A Linkam CAP500 heating stage was used to control the temperatures of the optical cells containing UO_2SO_4 solutions (25–420 °C). The temperature of the stage was calibrated with the melting temperatures of n-hexadecane (18.17 °C), sulfur (119 °C), and NaNO_3 (306.8 °C). This stage provided a good thermal stability (± 0.1 °C) with negligible temperature gradients (<1 °C within 15 mm). To accurately measure the temperature for the occurrence of liquid-liquid immiscibility, the heating rates were 5 °C/min at temperatures ≤ 250 °C and 1 °C/min at temperatures > 250 °C. A

microscope with 10 \times and 20 \times Olympus objectives was used to observe the phase behavior of the UO₂SO₄–H₂O system in the investigated temperature and pressure ranges.

Raman spectra of the $\nu_1(\text{UO}_2^{2+})$, $\nu_1(\text{SO}_4^{2-})$, and OH stretching [$\nu_s(\text{H}_2\text{O})$] bands were collected using a high resolution Raman spectrometer (LabRam HR, Jobin-Yvon Horiba). The spectra were collected using a frequency doubled Nd: YAG laser excitation with wavelength of 532.06 nm. The Raman spectrometer was equipped with air cooled CCD-detector (1024 \times 256 pixel, -70 °C), a long working distance objective (Olympus, 50 \times) and a 1800-groove/mm grating. The resolution of the Raman spectrometer is about 1.0 cm⁻¹. The laser power on the sample surface is about 9.5 mW. The $\nu_1(\text{UO}_2^{2+})$ and $\nu_1(\text{SO}_4^{2-})$ spectra were collected from 600 cm⁻¹ to 1400 cm⁻¹, and spectra for the $\nu_s(\text{H}_2\text{O})$ band were obtained from 2600 cm⁻¹ to 3900 cm⁻¹. The acquisition time was 40–240 s with three accumulations. The 1000.7 cm⁻¹ peak of benzonitrile (McCreery Research Group) was used to calibrate the wavenumbers of the collected spectra [24].

To characterize the speciation and relevant ion interaction in the UO₂SO₄–H₂O system at high temperatures, the PeakFit v. 4.0 program (AISN Software Inc.) was used to fit the spectra of the $\nu_1(\text{UO}_2^{2+})$ band. The spectra were treated with a Lorentz-Gaussian model, a linear baseline and 0.5 % smoothing.

3. Results and discussion

3.1. Liquid-liquid immiscibility

The phase behaviors of 1.04 mol/kg UO₂SO₄ in the optical cell were illustrated

in Fig. 1. At temperatures above 287.2 °C, a new liquid phase was separated from the aqueous phase at saturated vapor pressure (Figs. 1a, b). The new liquid phase was composed of a series of immiscible droplets scattering in the aqueous phase. Previous studies showed that the new liquid phase is rich in UO_2SO_4 , whereas the coexisting aqueous phase is poor in UO_2SO_4 [10]. For the ease of description, these two liquid phases were termed as U_{rich} and U_{poor} phases, respectively. As shown in Figs. 1c and d, U_{rich} droplets converged and the volume of a single U_{rich} droplet increased upon heating. During subsequent heating, the volume of the vapor phase decreased with increasing temperature, and homogenized into the U_{poor} phase at 362.5 °C (Figs. 1e~g). Then, the U_{rich} and U_{poor} phases were heated to 420 °C along an isochoric curve, assuming that the volume of the FSCL does not change. At temperatures above 350 °C, the property of the U_{poor} phase is very close to that of pure water due to its extremely low UO_2SO_4 concentration [10]. Secoy observed the critical temperature in the U_{poor} phase at *ca.* 374.0–374.4 °C [8]. Therefore, U_{rich} phase was converted to supercritical water (SCW) at temperatures above 374 °C and the U_{rich} phase and SCW coexisted at temperatures up to 420 °C. Figs. 1i~l show the near critical homogenization between U_{rich} and U_{poor} phases during cooling; volume of the U_{rich} phase increased and the $\text{U}_{\text{rich}}\text{--}\text{U}_{\text{poor}}$ phase boundary disappeared gradually with decreasing temperature.

Since liquid-liquid immiscibility is undesirable in homogenous reactors using UO_2SO_4 ($\text{H}_2\text{O}/\text{D}_2\text{O}$) solutions as fuels [10], many experimental observations were carried out to describe the phase boundaries of the two immiscible liquids under saturation pressures or hydrostatic pressures [9, 12]. As shown in Fig. 2 and Table 1,

the lowest temperature for the occurrence of liquid-liquid immiscibility is 285.8 ± 0.5 °C for 0.54 mol/kg UO_2SO_4 solution; the temperature for the separation of a new liquid phase decreases with increasing UO_2SO_4 concentration in more dilute solutions, whereas increases with increasing UO_2SO_4 concentration in more concentrated solutions. For aqueous solution, the lower critical solution temperature (LCST) is the low boundary temperature for the separation of new liquid phase(s) from the homogenous aqueous phase. Although several studies observed the LCST phenomena in the $\text{UO}_2\text{SO}_4\text{-H}_2\text{O}$ system, disagreement exists (Fig. 2). Our observations show that the LCST is at 285.8 ± 0.5 °C, which is almost the same as that reported by Marshall and Gill (286 °C) [12].

Unlike previous observations [9, 11], the liquid-liquid immiscibility was found to be fairly stable in aqueous UO_2SO_4 solutions because no precipitates were observed in all the investigated samples at temperatures up to 420 °C. To investigate the possible changes in the thermodynamic properties of the $\text{UO}_2\text{SO}_4\text{-H}_2\text{O}$ system, Yang and Pitzer conducted theoretical calculations at temperatures close to the critical temperature of the liquid-liquid immiscibility [27]. According to their calculation, liquid-liquid immiscibility was expected to occur in 2-2 electrolyte solution with considerable solubility at 250–300 °C. The absence of liquid-liquid immiscibility in most 2-2 electrolyte solutions was ascribed to the remarkably reduced solubilities at temperatures above 77–127 °C [27]. This result can explain the unusual phase behavior in aqueous UO_2SO_4 solution, because $\text{UO}_2\text{SO}_4\cdot\text{H}_2\text{O}$ exhibits exceptionally high solubility at elevated temperatures (7.75 mol/kg at 287 °C, [28]). However, it

cannot explain the formation of liquid-liquid immiscibility in aqueous MgSO₄ solution at temperatures above 260 °C [24] because the solubility of kieserite (MgSO₄·H₂O) was reported to be significantly reduced at temperatures above 200 °C [29].

Marshall and Gill observed the liquid-liquid immiscibility in aqueous solutions at pressures up to 180 MPa and proposed that the liquid-liquid immiscibility temperature increases approximately linearly with pressure [12]. They noticed the relationship between the complex ion association and the liquid-liquid immiscibility. Considering liquid-liquid immiscibility is common in organic-bearing solutions, the uranyl–sulfate ion association was suggested to create an organic-like aqueous solution favoring the separation of a new liquid phase at elevated temperatures [12]. In fact, it has been accepted that the LCST phenomenon characterizes polymer solution [30–31]. Therefore, our observations of the LCST phenomena support the strong ion association in aqueous UO₂SO₄ solution at high temperatures.

3.2. Ion association between UO₂²⁺ and SO₄²⁻

The free uranyl ion (UO₂²⁺)_{aq} displays a symmetric stretching mode (ν_1) at *ca.* 870 cm⁻¹ [15–16, 18, 32–33]. Unassociated SO₄²⁻_(aq) is characterized by a prominently symmetric mode (ν_1) at *ca.* 980 cm⁻¹ [34]. Both $\nu_1(\text{UO}_2^{2+})$ and $\nu_1(\text{SO}_4^{2-})$ bands can serve as indicators to investigate the complexation in the UO₂SO₄–H₂O system because these two Raman bands are sensitive to changes in coordination environment [13–14, 17–23].

As shown in Fig. 3, the U_{rich} phase is characterized by strong $\nu_1(\text{UO}_2^{2+})$ and

$\nu_1(\text{SO}_4^{2-})$ bands, whereas those bands in the U_{poor} phase are weak. Figs. 4 and 5 show the Raman spectra of $\nu_1(\text{UO}_2^{2+})$ and $\nu_1(\text{SO}_4^{2-})$ bands in 0.54 mol/kg UO₂SO₄ at temperatures from 25 to 420 °C. In the aqueous phase (≤ 275 °C), no obvious change in the peak position and peak width of the $\nu_1(\text{UO}_2^{2+})$ band has been observed (Fig. 4a). However, the symmetry of the $\nu_1(\text{UO}_2^{2+})$ band increases with increasing temperature. The $\nu_1(\text{UO}_2^{2+})$ band shows three components at *ca.* 870 cm⁻¹ (C_{870}), 860 cm⁻¹ (C_{860}) and 852 cm⁻¹ (C_{852}) (Fig. 4a and Supplementary Material). These three $\nu_1(\text{UO}_2^{2+})$ sub-bands have been observed in aqueous UO₂SO₄ solutions with sulfate/uranyl ratio ranging from 5 to 600 at room temperature [13] and can be assigned to UO₂²⁺, UO₂SO₄⁰, and UO₂(SO₄)²⁻, respectively [13–14]. With increasing temperature, the relative peak height of C_{860} and C_{852} increases whereas that of C_{870} decreases (Fig. 4a). Meanwhile, the C_{870} component shifts to higher wavenumber with the rise in temperature. After the occurrence of the liquid-liquid immiscibility, the higher-wavenumber shift of C_{870} component in the U_{rich} phase is more obvious (Fig. 4a). The $\nu_1(\text{UO}_2^{2+})$ bands become more symmetric and shift to higher wavenumber with increasing temperature; *ca.* 3 cm⁻¹ higher-wavenumber shift was observed from 300 to 420 °C. The intensity of C_{870} sub-band decreases with increasing temperature and cannot be detected at temperatures above 320 °C (Fig. 4a). This result indicates that uranyl complexes are the dominant uranyl species in the U_{rich} phase. The $\nu_1(\text{UO}_2^{2+})$ bands of the U_{rich} and U_{poor} phases at the same temperature were also compared to investigate the speciation differences. In the U_{poor} phase, the shape of $\nu_1(\text{UO}_2^{2+})$ band is similar to that for aqueous phase (Supplementary Material);

deconvolution of the $\nu_1(\text{UO}_2^{2+})$ band shows the presence of UO_2^{2+} , UO_2SO_4^0 and $\text{UO}_2(\text{SO}_4)_2^{2-}$ at *ca.* 870 cm^{-1} , 860 cm^{-1} and 852 cm^{-1} , respectively. However, the $\nu_1(\text{UO}_2^{2+})$ band of the U_{rich} phase is characterized by two $\nu_1(\text{UO}_2^{2+})$ sub-bands at *ca.* 864 cm^{-1} and 854 cm^{-1} , respectively, shifting to higher wavenumber compared with those in the U_{poor} phase (Supplementary Material). Nguyen-Trung et al. observed the higher-wavenumber shift of $\nu_1(\text{UO}_2^{2+})$ bands in aqueous uranyl perchlorate solutions [13]. The higher-wavenumber shift of the $\nu_1(\text{UO}_2^{2+})$ band was ascribed to the weakness in the solvation shell of UO_2^{2+} [13]. Our results show that the higher-wavenumber shift of the $\nu_1(\text{UO}_2^{2+})$ bands in aqueous phase at high temperatures may also arise from the complex $\text{UO}_2^{2+}\text{--SO}_4^{2-}$ association. However, further experimental observation and theoretical simulation are needed to make clear assignments of the $\nu_1(\text{UO}_2^{2+})$ sub-bands in concentrated aqueous uranyl solutions, especially at high temperatures.

As to the $\nu_1(\text{SO}_4^{2-})$ bands, the spectrum shapes are more complex. As shown in Fig. 4b, the wavenumber of $\nu_1(\text{SO}_4^{2-})$ band shifts from *ca.* 980 cm^{-1} to 1020 cm^{-1} when the sample was heated from $25 \text{ }^\circ\text{C}$ to $420 \text{ }^\circ\text{C}$. Meanwhile, the $\nu_1(\text{SO}_4^{2-})$ band becomes broader with increasing temperature. The symmetry of the $\nu_1(\text{SO}_4^{2-})$ band decreases in the homogeneous aqueous phase, whereas increases in the U_{rich} phase with the rise of temperature. At temperatures from 25 to $150 \text{ }^\circ\text{C}$, three $\nu_1(\text{SO}_4^{2-})$ components centered at *ca.* 980 cm^{-1} , 992 cm^{-1} and 1002 cm^{-1} have been identified (Fig. 4b). In the U_{rich} phase, another two $\nu_1(\text{SO}_4^{2-})$ components at *ca.* 1015 cm^{-1} and 1028 cm^{-1} can be recognized (Fig. 4b). Due to the complex shape of the $\nu_1(\text{SO}_4^{2-})$

spectra, no deconvolution has been carried out. As far as know, descriptions of the $\nu_1(\text{SO}_4^{2-})$ spectra in aqueous UO_2SO_4 solutions has rarely been documented. According to the researches on the Raman $\nu_1(\text{SO}_4^{2-})$ band in aqueous MgSO_4 solution, the $\nu_1(\text{SO}_4^{2-})$ component at *ca.* 980 cm^{-1} should arise from unassociated SO_4^{2-} , whereas the $\nu_1(\text{SO}_4^{2-})$ components at *ca.* 992 cm^{-1} and 1002 cm^{-1} may represent the contribution from contact ion pair and triple ion pair, respectively [20–24]. However, it's difficult to make clear assignments for the $\nu_1(\text{SO}_4^{2-})$ components at *ca.* 1015 and 1028 cm^{-1} . It has been reported that the $\nu_1(\text{SO}_4^{2-})$ band becomes broader and the wavenumber increases with the increase of the length of inner-sphere ion pairs in aqueous MgSO_4 solution [21, 23, 35–36]. Considering the obvious higher-wavenumber shift of the $\nu_1(\text{SO}_4^{2-})$ band (Fig. 4b), the ion association should be more complex than those derived from analyses of the $\nu_1(\text{UO}_2^{2+})$ bands in low temperature $\text{UO}_2(\text{SO}_4)_2$ solutions. Therefore, ions and/or simple ion pairs should transform to complex ion pairs as well as ion pair chain structures (polymers) in aqueous UO_2SO_4 solution at high temperatures. Another band at *ca.* 1044 cm^{-1} was observed in the U_{rich} phase (Fig. 4b); it might be in association with the $\nu_3(\text{SO}_4^{2-})$ mode of $\text{UO}_2^{2+}-\text{SO}_4^{2-}$ ion pairs [16], which was also observed in aqueous phase (Fig. 4b). It should be noted that the Raman signals of $\nu_1(\text{SO}_4^{2-})$ bands are very weak in the U_{poor} phase and were not further studied in this study (Fig. 5).

In addition to the $\nu_1(\text{UO}_2^{2+})$ and $\nu_1(\text{SO}_4^{2-})$ bands, the asymmetric stretching band of UO_2^{2+} (ν_a) was also identified at *ca.* 960 cm^{-1} (Fig. 4b) [16]. It shifts from *ca.* 960 cm^{-1} to 950 cm^{-1} at temperatures from 25 °C to 275 °C; the lower-wavenumber shift

should be ascribed to the ion association between UO_2^{2+} and SO_4^{2-} [18, 33]. The $\nu_a(\text{UO}_2^{2+})$ band is weak in the U_{rich} phase and cannot be detected at temperatures above 350 °C. For HSO_4^- , the intensity of $\nu_1(\text{HSO}_4^-)$ band increases with increasing temperature in aqueous UO_2SO_4 solution, indicating an increase of hydrolysis of uranyl with increasing temperature (Fig. 4b). However, in the U_{rich} phase, the $\nu_1(\text{HSO}_4^-)$ band is not obvious. Previous studies reported that $\text{UO}_2^{2+}\text{--}\text{SO}_4^{2-}$ ion pairing is more stable than that between UO_2^{2+} and HSO_4^- [13–14]. In some cases, HSO_4^- was even considered to be non-complexing anion at high temperature [37]. As a result, the left UO_2^{2+} in the U_{poor} phase coordinated with SO_4^{2-} to form stable $\text{UO}_2^{2+}\text{--}\text{SO}_4^{2-}$ ion pairs. This process was promoted by the transformation of HSO_4^- to SO_4^{2-} .

In summary, *in situ* Raman spectroscopic description of the liquid-liquid immiscibility in $\text{UO}_2\text{SO}_4\text{--H}_2\text{O}$ system supports previous speculations that the ion pairing between UO_2^{2+} and SO_4^{2-} increases with increasing temperature [12, 38]. A decrease of the dielectric constant of water with increasing temperature, especially under supercritical conditions, favors the strong $\text{UO}_2^{2+}\text{--}\text{SO}_4^{2-}$ ion association to form complex ion pairs, even polymer structures.

3.3. UO_2SO_4 concentration of the immiscible fluids

Previous studies suggested that the integrated Raman intensity (peak area) ratio between Raman active species and water could be used to indicate the concentration of corresponding species in water; Raman peak areas are proportional to the number of species in the analyzed volume [39]. In aqueous UO_2SO_4 solution, both UO_2^{2+} and SO_4^{2-} are Raman active, among which the $\nu_1(\text{UO}_2^{2+})$ band is stronger. Theoretically,

the peak area ratio between $\nu_1(\text{UO}_2^{2+})$ and $\nu_s(\text{H}_2\text{O})$ bands ($A_{\text{uranyl}}/A_{\text{water}}$) can provide information on the content of uranyl in the U_{rich} and U_{poor} phases. Similarly, the content of sulfate can also be measured by calculating the peak area ratio between $\nu_1(\text{SO}_4^{2-})$ and $\nu_s(\text{H}_2\text{O})$ bands. However, variation of the relative differential scattering cross sections with temperature [40] and lack of calibration of our Raman system for quantitative analyses prevent accurate measurements of the uranyl concentrations of the immiscible liquids. In this study, the $A_{\text{uranyl}}/A_{\text{water}}$ ratios were employed to qualitatively indicate the variation of uranyl contents with the rise of temperature in both immiscible liquids. The changes of sulfate content were not further investigated due to the relatively lower Raman intensity of $\nu_1(\text{SO}_4^{2-})$ bands, especially in the U_{poor} phase (Fig. 5).

Fig. 6 shows the relationship between the $A_{\text{uranyl}}/A_{\text{water}}$ ratio and temperature in immiscible U_{rich} and U_{poor} phases for 0.54 mol/kg UO_2SO_4 . The $A_{\text{uranyl}}/A_{\text{water}}$ ratio increases with the rise of temperature in the U_{rich} phase, indicating that U_{rich} phase becomes more concentrated as temperature increases. In the U_{poor} phase, the $A_{\text{uranyl}}/A_{\text{water}}$ ratio is obviously reduced with the increase of temperature, indicating a decrease in the UO_2SO_4 contents with increasing temperature. At temperatures above 350 °C, the $A_{\text{uranyl}}/A_{\text{water}}$ ratio is approaching zero in the U_{poor} phase, indicating that the UO_2SO_4 concentration is very low. As shown in Fig. 3, it is obvious that the Raman intensities of both $\nu_1(\text{UO}_2^{2+})$ and $\nu_1(\text{SO}_4^{2-})$ bands are strong in the U_{rich} phase in the investigated temperature range, whereas those in the U_{poor} phase decreases with increasing temperature. The signal of $\nu_1(\text{UO}_2^{2+})$ bands in the U_{poor} phase cannot even

be detected at temperatures above 370 °C (Fig. 5). The above observations can be well compared with those reported by Jones and Marshall [10]; they found that, with temperature increased from 300 to 350 °C, the U_{rich} phase became more concentrated and the U_{poor} phase became more dilute. It is well known that both UO₂²⁺ and SO₄²⁻ are surrounded by strong hydration shells in aqueous solutions. X-ray diffraction study shows that UO₂²⁺ is surrounded by five inner-sphere water molecules and the U-O_w distance is about 0.241 nm [41]. Vchirawongkwin et al. suggested that the coordination number of SO₄²⁻ is about 11–12 water molecules based on molecular dynamics simulation and X-ray scattering investigation [42]. As a result, the hydration of UO₂²⁺ and SO₄²⁻ cannot be maintained in concentrated U_{rich} phase. In other words, UO₂²⁺ and SO₄²⁻ are highly associated in the U_{rich} phase. This is in line with previous studies suggesting that the ion association increases with increasing sulfate concentration [21, 43].

It is noted that the Raman signal of $\nu_1(\text{HSO}_4^-)$ (*ca.* 1050 cm⁻¹) can be observed in the U_{poor} phase at 370 °C, whereas the $\nu_1(\text{UO}_2^{2+})$ band is weak (Fig. 5). In the $\nu_1(\text{UO}_2^{2+})$ -intensity normalized spectra of the $\nu_1(\text{SO}_4^{2-})$ bands, it is obvious that the U_{poor} phase was characterized by a predominant $\nu_1(\text{HSO}_4^-)$ band, which was even not observed in the U_{rich} phase (Fig. 7). Considered the strong U-O bonding [44] but weak $\nu_1(\text{UO}_2^{2+})$ signal in the U_{poor} phase (Fig. 5a), the relatively higher $\nu_1(\text{HSO}_4^-)$ intensity indicates that the U_{poor} phase should be of excess HSO₄⁻. This observation can be well compared with the compositions of the immiscible liquids measured using quenching methods; Jones and Marshall found that the U_{poor} phase contained excess of HSO₄⁻

and the U_{rich} phase was about stoichiometric [10]. Therefore, uranyl and sulfate were preferentially accumulated in the U_{rich} phase. Meanwhile, the primary sulfate species in the U_{poor} phase was HSO₄⁻, especially at temperatures above 330 °C. However, unlike the continuous increasing of HSO₄⁻ concentration in the U_{poor} phase reported by Jones and Marshall [10], our results show that the Raman intensity of the $\nu_1(\text{HSO}_4^-)$ band in the U_{poor} phase increased with increasing temperature from 300 to 350 °C, and then started to decrease at temperatures above 360 °C; in SCW, the $\nu_1(\text{HSO}_4^-)$ band cannot be identified (Fig. 5). This can be ascribed to the relatively stronger ion interaction between UO₂²⁺ and SO₄²⁻ [13–14].

4. Conclusions

In this study, the liquid-liquid immiscibility in UO₂SO₄–H₂O system was observed at temperatures up to 420 °C. To investigate the possible changes in speciation or structure inducing the liquid-liquid immiscibility, in situ Raman spectra of the $\nu_1(\text{UO}_2^{2+})$, $\nu_1(\text{SO}_4^{2-})$, and $\nu_s(\text{HO}_2)$ bands were collected using a high resolution Raman spectrometer. Our results suggest that a reversible polymerization between uranyl and sulfate triggers the liquid-liquid immiscibility in UO₂SO₄–H₂O system. The evidences were summarized as follows:

(1) Temperatures for the occurrence of the liquid-liquid immiscibility were obtained using a new heating stage. The temperature-composition phase diagram of the UO₂SO₄–H₂O system is characterized by lower critical solution temperature phenomenon (LCST = 285.8±0.5 °C). The presence of LSCT is considered to be a characteristic phenomenon of polymer solution;

(2) In situ Raman spectra of the immiscible liquid phases in the UO₂SO₄–H₂O system were documented. Analyses of the $\nu_1(\text{UO}_2^{2+})$ and $\nu_1(\text{SO}_4^{2-})$ bands indicate that UO₂²⁺ and SO₄²⁻ were highly associated in the U_{rich} phase, whereas the UO₂²⁺–SO₄²⁻ association was weaker in the U_{poor} phase;

(3) Experiments were conducted to reflect the variation of the UO₂SO₄ concentration in the U_{rich} and U_{poor} phases by analyzing the peak area ratios between $\nu_1(\text{UO}_2^{2+})$ and $\nu_s(\text{HO}_2)$ bands. Results show that the U_{rich} phase was getting more concentrated with increasing temperature. In this case, the hydration of UO₂²⁺ and SO₄²⁻ cannot be maintained, which further implies the strong ion complexation in the U_{rich} phase.

Acknowledgments

The editor, Richard L. Smith, Dr. Gleb Pokrovski, and two anonymous reviewers are thanked for their careful reviews and constructive comments. This work was financially supported by National Natural Science Foundation of China (Grant Nos. 41573054, 41230312 and 41203045), the Knowledge Innovation Program (SIDSSE-201302), and the Hadal-trench Research Program (XDB06060100) of Chinese Academy of Sciences.

References

- [1] P. Kritzer, N. Boukis, E. Dinjus, Factors controlling corrosion in high-temperature aqueous solutions: a contribution to the dissociation and solubility data influencing corrosion processes, *J. Supercrit. Fluid* 15 (1999) 205–227.
- [2] M. Hodes, P.A., Marrone, G.T. Hong, K.A. Smith, J.W. Tester, Salt precipitation and scale control in supercritical water oxidation—Part A: fundamentals and research,

- J. Supercrit. Fluid 29 (2004) 265–288.
- [3] I. Leusbrock, S.J. Metz, G. Rexwinkel, G.F. Versteeg, The solubilities of phosphate and sulfate salts in supercritical water, J. Supercrit. Fluid 54 (2010) 1–8.
- [4] Y. Matsumoto, H. Harada, K. Yui, H. Uchida, K. Itatani, S. Koda, Raman spectroscopic study of aqueous alkali sulfate solutions at high temperature and pressure to yield precipitation, J. Supercrit. Fluid 49 (2009) 303–309.
- [5] M. Schubert, J.W. Regler, F. Vogel, Continuous salt precipitation and separation from supercritical water. Part 2. Type 2 salts and mixtures of two salts, J. Supercrit. Fluid 52 (2010) 113–124.
- [6] V.M. Valyashko, Phase behavior in binary and ternary water – salt systems at high temperatures and pressures, Pure Appl. Chem. 69 (1997) 2271–2280.
- [7] V.M. Valyashko, Phase equilibria in binary and ternary hydrothermal systems, in: V.M. Valyashko (Ed.), Hydrothermal Properties of Materials, Wiley, 2008. pp. 1–133.
- [8] C.H. Secoy, The system uranyl-sulfate-water. II. Temperature-concentration relationships above 250 °C, J. Am. Chem. Soc. 72 (1950) 3343–3345.
- [9] F.E. Clark, J.S. Gill, R. Slusher, C.H. Secoy, Phase behavior of the system UO_2SO_4 - CuSO_4 - H_2SO_4 - H_2O at elevated temperatures, J. Chem. Eng. Data 4 (1959) 12–15.
- [10] E.V. Jones, W.L. Marshall, Aqueous systems at high temperature-IV: Compositions of light- and heavy-liquid phases in the systems UO_3 - SO_3 - H_2O , UO_3 - SO_3 - D_2O , J. Inorg. Nucl. Chem. 23 (1961) 287–293.
- [11] W.L. Marshall, E.V. Jones, G.M. Hebert, F.J. Smith, Aqueous systems at high temperature-VII: Liquid-liquid immiscibility and critical phenomena in the systems UO_3 - SO_3 - H_2O , UO_3 - SO_3 - D_2O and CuO - SO_3 - D_2O , 270–430 °C, J. Inorg. Nucl. Chem. 24 (1962) 995–1000.
- [12] W.L. Marshall, J.S. Gill, Effects of pressure on liquid-liquid immiscibility of high temperature aqueous solution mixtures of uranyl sulfate and sulfuric acid, 280–450 °C, 75–1800 bars, J. Inorg. Nucl. Chem. 36 (1974) 2303–2312.
- [13] C. Nguyen-Trung, G.M. Begun, D.A. Palmer, Aqueous uranium complexes. 2. Raman spectroscopic study of the complex formation of the dioxouranium (VI) ion

- with a variety of inorganic and organic ligands, *Inorg. Chem.* 31 (1992) 5280–5287.
- [14] A. Burneau, M. Tazi, G. Bouzat, Raman spectroscopic determination of equilibrium constants of uranyl sulphate complexes in aqueous solutions, *Talanta* 39 (1992) 743–748.
- [15] M. Gál, P.L. Googin, J. Mink, Mid-, Far-infrared and Raman spectra of uranyl complexes in aqueous solutions, *J. Mol. Struct.* 114 (1984) 459–462.
- [16] M. Gál, P.L. Goggin, J. Mink, Vibrational spectroscopic studies of uranyl complexes in aqueous and non-aqueous solutions, *Spectrochim. Acta* 48A (1992) 121–132.
- [17] L.M. Toth, G.M. Begun, Raman spectra of uranyl ion and its hydrolysis products in aqueous nitric acid, *J. Phys. Chem.* 85 (1981) 547–549.
- [18] S.P. Pasilis, J.E. Pemberton, Speciation and coordination chemistry of uranyl(VI)-citrate complexes in aqueous solution, *Inorg. Chem.* 42 (2003) 6793–6800.
- [19] M. Dargent, J. Dubessy, L. Truche, E.F. Bazarkina, C. Nguyen-Trung, P. Robert, Experimental study of uranyl(VI) chloride complex formation in acidic LiCl aqueous solutions under hydrothermal conditions ($T=21\text{ }^{\circ}\text{C}$ – $350\text{ }^{\circ}\text{C}$, P_{sat}) using Raman spectroscopy, *Eur. J. Mineral.* 25 (2013) 765–775.
- [20] Y.-H. Zhang, C.K. Chan, Study of contact ion pairs of supersaturated magnesium sulfate solutions using Raman scattering of levitated single droplets, *J. Phys. Chem. A* 104 (2000) 9191–9196.
- [21] W.W. Rudolph, G. Irmer, G.T. Hefter, Raman spectroscopic investigation of speciation in $\text{MgSO}_4(\text{aq})$, *Phys. Chem. Chem. Phys.* 5 (2003) 5253–5261.
- [22] R. Buchner, W.W. Rudolph, G.T. Hefter, Comment on “Dynamic ion association in aqueous solutions of sulfate” [*J. Chem. Phys.* 123, 034508 (2005)], *J. Chem. Phys.* 124 (2006) 247101, 1–3.
- [23] S. Jahn, C. Schmidt, Speciation in aqueous MgSO_4 fluids at high pressures and high temperatures from ab Initio molecular dynamics and Raman spectroscopy, *J. Phys. Chem. B* 114 (2010) 15565–15572.
- [24] X. Wang, I-M. Chou, W. Hu, R.C. Burruss, In situ observations of liquid-liquid

- phase separation in aqueous MgSO₄ solutions: Geological and geochemical implications, *Geochim. Cosmochim. Acta* 103 (2013) 1–10.
- [25] I-M. Chou, Y. Song, R.C. Burruss, A new method for synthesizing fluid inclusions in fused silica capillaries containing organic and inorganic material, *Geochim. Cosmochim. Acta* 72 (2008) 5217–5231.
- [26] J. Jin, J. Wang, Y. Shen, C. Lin, Z. Pan, I-M. Chou, Visual and Raman spectroscopic observations of hot compressed water oxidation of guaiacol in fused silica capillary reactors, *J. Supercrit. Fluid* 95 (2014) 546–552.
- [27] J.-Z. Yang, K.S. Pitzer, Thermodynamics of aqueous uranyl sulfate to 559 K, *J. Solution Chem.* 18 (1989) 189–199.
- [28] C. Secoy, The system uranyl sulfate-water. I. Temperature-concentration relationships below 300 °C, *J. Am. Chem. Soc.* 70 (1948) 3450–3452.
- [29] H.L. Robson, The system MgSO₄-H₂O from 68 to 240 °, *J. Am. Chem. Soc.* 49 (1927) 2772–2783.
- [30] P. Paricaud, A. Galindo, G. Jackson, Understanding liquid-liquid immiscibility and LCST behaviour in polymer solutions with a Wertheim TPT1 description, *Mol. Phys.* 101 (2003) 2575–2600.
- [31] K. Gong, B.D. Marshall, W.G. Chapman, Modeling lower critical solution temperature behavior of associating polymer brushes with classical density functional theory, *J. Chem. Phys.* 139 (2013) 094904, 1–8.
- [32] J.I. Bullock, Raman and Infrared spectroscopic studies of the uranyl ion: the symmetric stretching frequency, force constants, and bond lengths, *J. Chem. Soc. A* (1969) 781–784.
- [33] F. Quilès, A. Burneau, Infrared and Raman spectra of uranyl(VI) oxo-hydroxo complexes in acid aqueous solutions: a chemometric study, *Vib. Spectrosc.* 23 (2000), 231–241.
- [34] J.L. Dong, X.H. Li, L.J. Zhao, H. Xiao, F. Wang, X. Guo, Y. Zhang, Raman observation of the interaction between NH₄⁺, SO₄²⁻, and H₂O in supersaturated (NH₄)₂SO₄ droplets, *J. Phys. Chem. B* 111 (2007) 12170–12176.
- [35] F. Rull, F. Sobrón, Band profile analysis of the Raman spectra of sulfate ions in

- aqueous solutions, *J. Raman Spectrosc.* 25 (1994) 693–698.
- [36] X. Zhang, Y. Zhang, Q. Li, Ab initio studies on the chain of contact ion pairs of magnesium sulfate in supersaturated state of aqueous solution. *J. Mol. Struct. (Theochem.)* 594 (2002) 19–30.
- [37] W.W. Rudolph, R. Mason, Study of aqueous $\text{Al}_2(\text{SO}_4)_3$ solution under hydrothermal conditions: sulfate ion pairing, hydrolysis, and formation of hydronium alunite, *J. solution chem.* 30(6) (2001) 527–548.
- [38] J. Neufeld, S. Skanthakumar, L. Soderholm, Structure of the $\text{UO}_2^{2+}\text{-SO}_4^{2-}$ ion pair in aqueous solution, *Inorg. Chem.* 43 (2004) 2422–2426.
- [39] J. Dubessy, D. Geisler, C. Kosztolanyi, M. Vernet, The determination of sulfate in fluid inclusions using the M.O.L.E. Raman microprobe: Application to a Keuper halite and geochemical consequences, *Geochim. Cosmochim. Acta* 47 (1983) 1–10.
- [40] V.G. Baonza, F. Rull, J. Dubessy, Raman spectroscopy of gases, water and other geological fluids, in: J. Dubessy, C.-C. Caumon, F. Rull (Eds.), *Raman Spectroscopy Applied to Earth Sciences and Cultural Heritage*, EMU Notes in Mineralogy, The European Mineralogical Union and the Mineralogical Society of Great Britain, London, 2012. pp. 279–320. [41] M. Åberg, D. Ferri, J. Glaser, I. Grenthe, Structure of the hydrated dioxouranium(VI) ion in aqueous solution. An X-ray diffraction and ^1H NMR study, *Inorg. Chem.* 22 (1983) 3986–3989.
- [42] V. Vchirawongkwin, B.M. Rode, I. Persson, Structure and dynamics of sulfate ion in aqueous solution—An ab initio QMCF MD simulation and large angle X-ray scattering study, *J. Phys. Chem. B* 111(2007) 4150–4155.
- [43] H. Zhang, Y.-H. Zhang, F. Wang, Theoretical understanding on the $\nu_1\text{-SO}_4^{2-}$ band perturbed by the formation of magnesium sulfate ion pairs, *J. Comput. Chem.* 30 (2009) 493–503.
- [44] K.E. Gutowski, D.A. Dixon, Predicting the energy of water exchange reaction and free energy of solvation for the uranyl ion in aqueous solution, *J. Phys. Chem. A* 110 (2006) 8840–8856.

Figure captions

Fig. 1. Photos showing the liquid-liquid immiscibility in 1.04 mol/kg UO_2SO_4 solution at elevated temperatures and pressures. A, V, U_{rich} , U_{poor} , and SCW represent aqueous phase, vapor phase, UO_2SO_4 -rich phase, UO_2SO_4 -poor phase, and supercritical water, respectively.

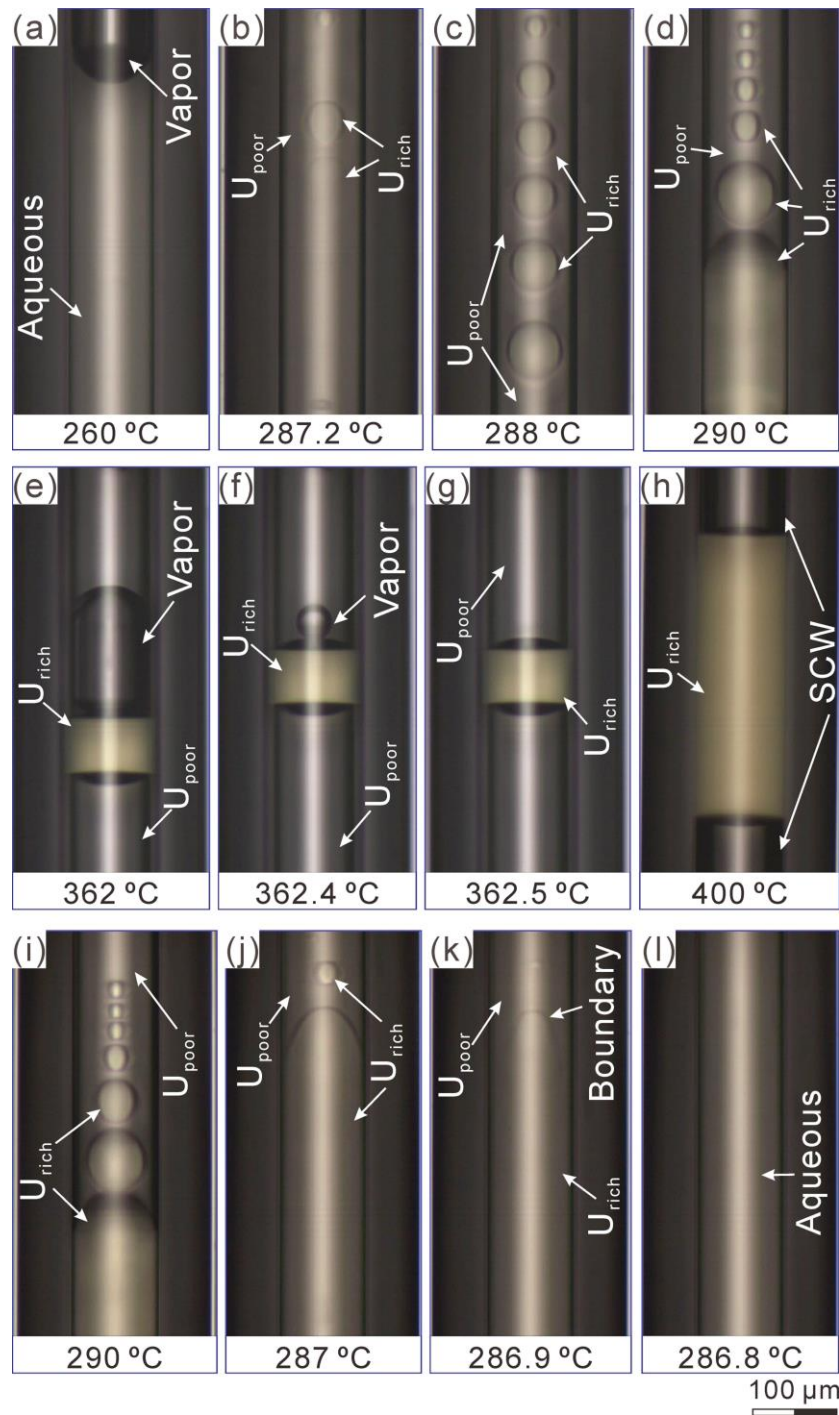


Fig. 2. Temperature-composition diagram of the $\text{UO}_2\text{SO}_4-\text{H}_2\text{O}$ system showing the boundary temperatures for the occurrence of liquid-liquid immiscibility of specific UO_2SO_4 solutions at saturated vapor pressures. The plotted data are from Table 1 (squares) and those documented in [8, diamonds], [9, triangles], [11, inverted triangles] and [12, circles].

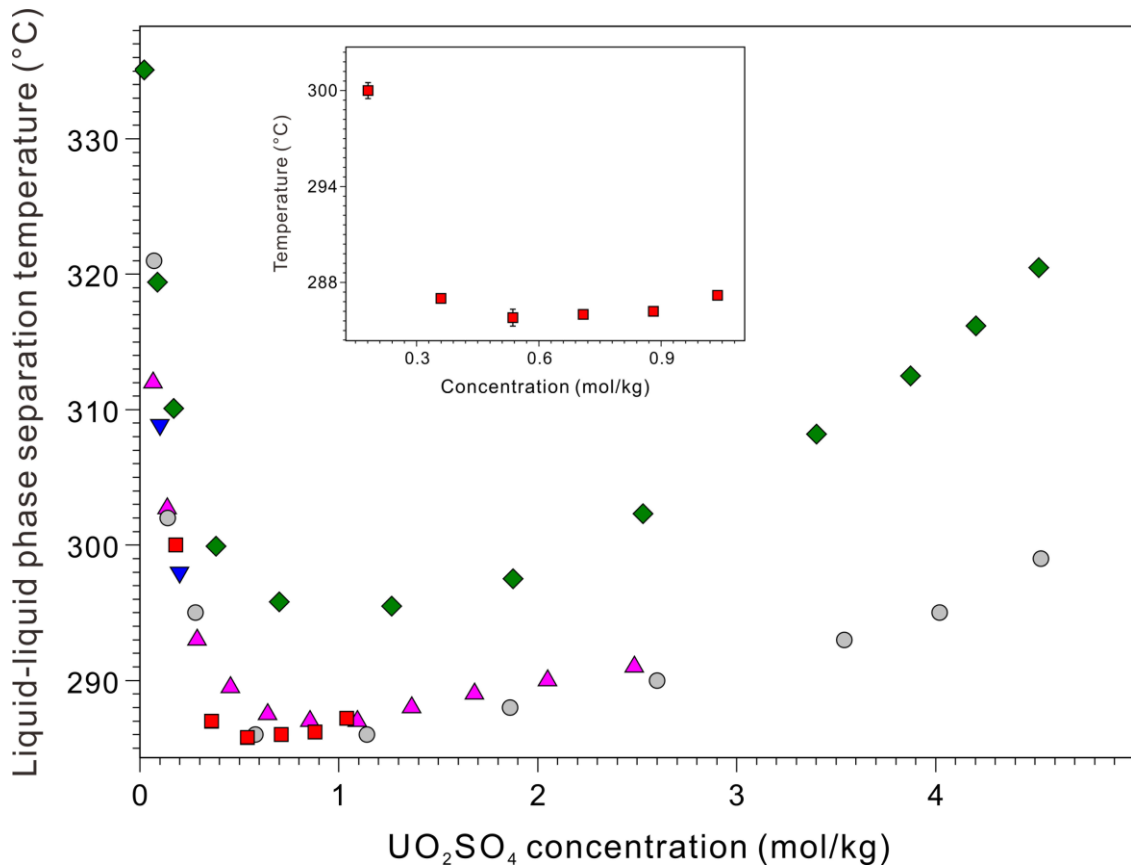


Fig. 3. In situ Raman spectroscopic analyses for immiscible U_{rich} and U_{poor} liquids in 1.04 mol/kg UO₂SO₄ solution. (a) U_{rich} liquid at 350 °C; (b) U_{poor} liquid at 350 °C; (c) U_{rich} liquid at 300 °C; and (d) U_{poor} liquid at 300 °C.

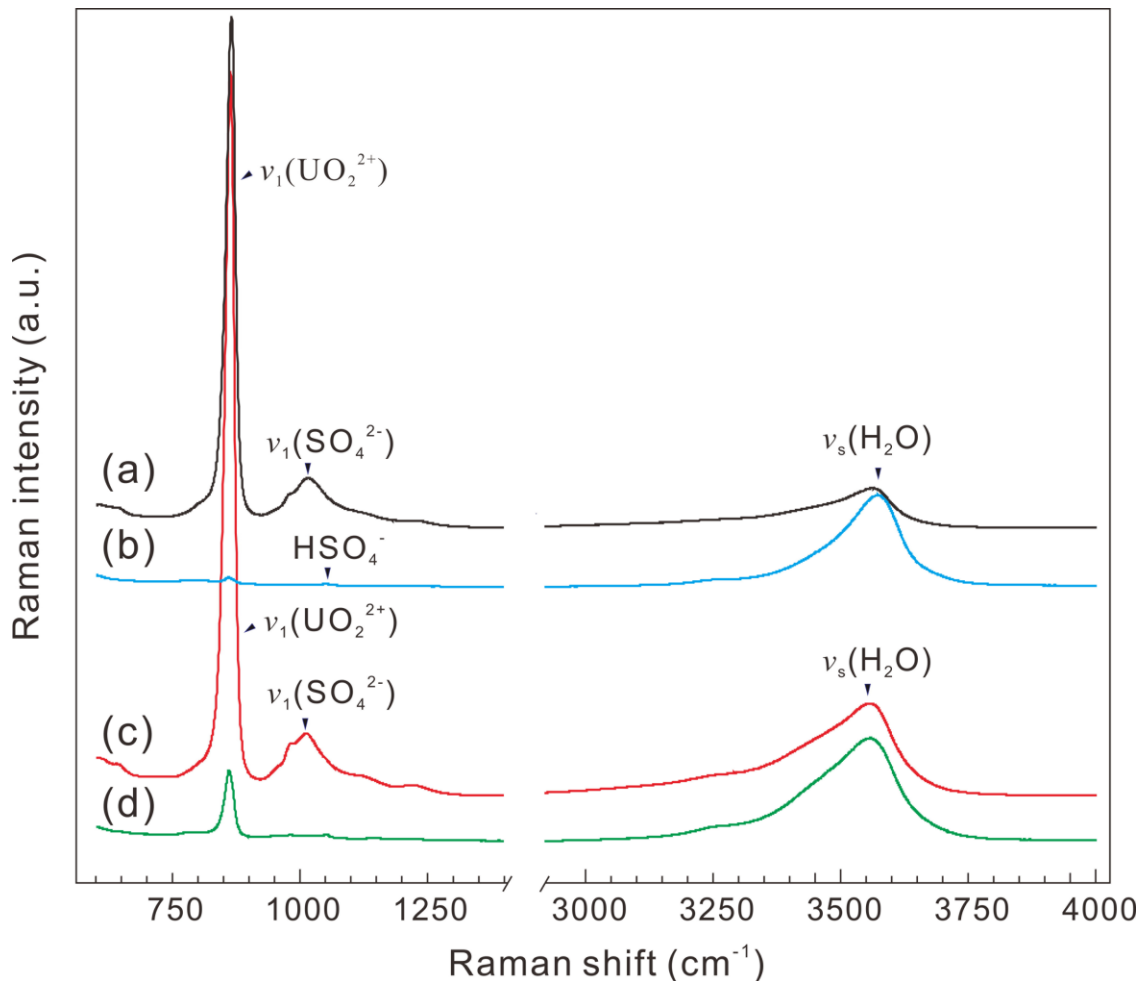


Fig. 4. Raman spectra of $\nu_1(\text{UO}_2^{2+})$ (a) and $\nu_1(\text{SO}_4^{2-})$ (b) bands in aqueous and U-rich liquid phases of 0.54 mol/kg UO_2SO_4 from 25 to 420 °C.

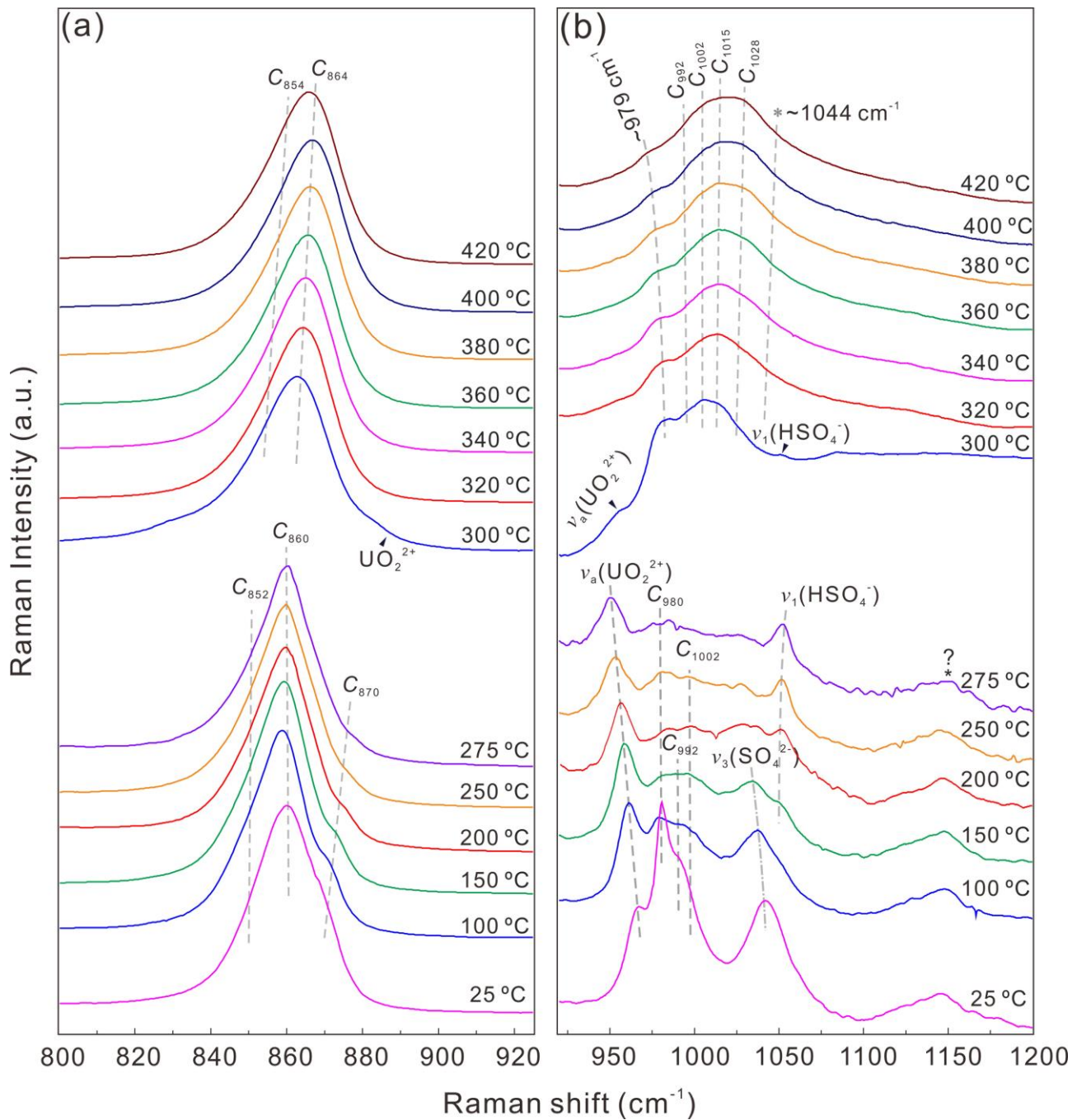


Fig. 5. Raman spectra of uranyl and sulfate bands in U_{poor} liquid of 0.54 mol/kg UO₂SO₄ from 300 to 420 °C.

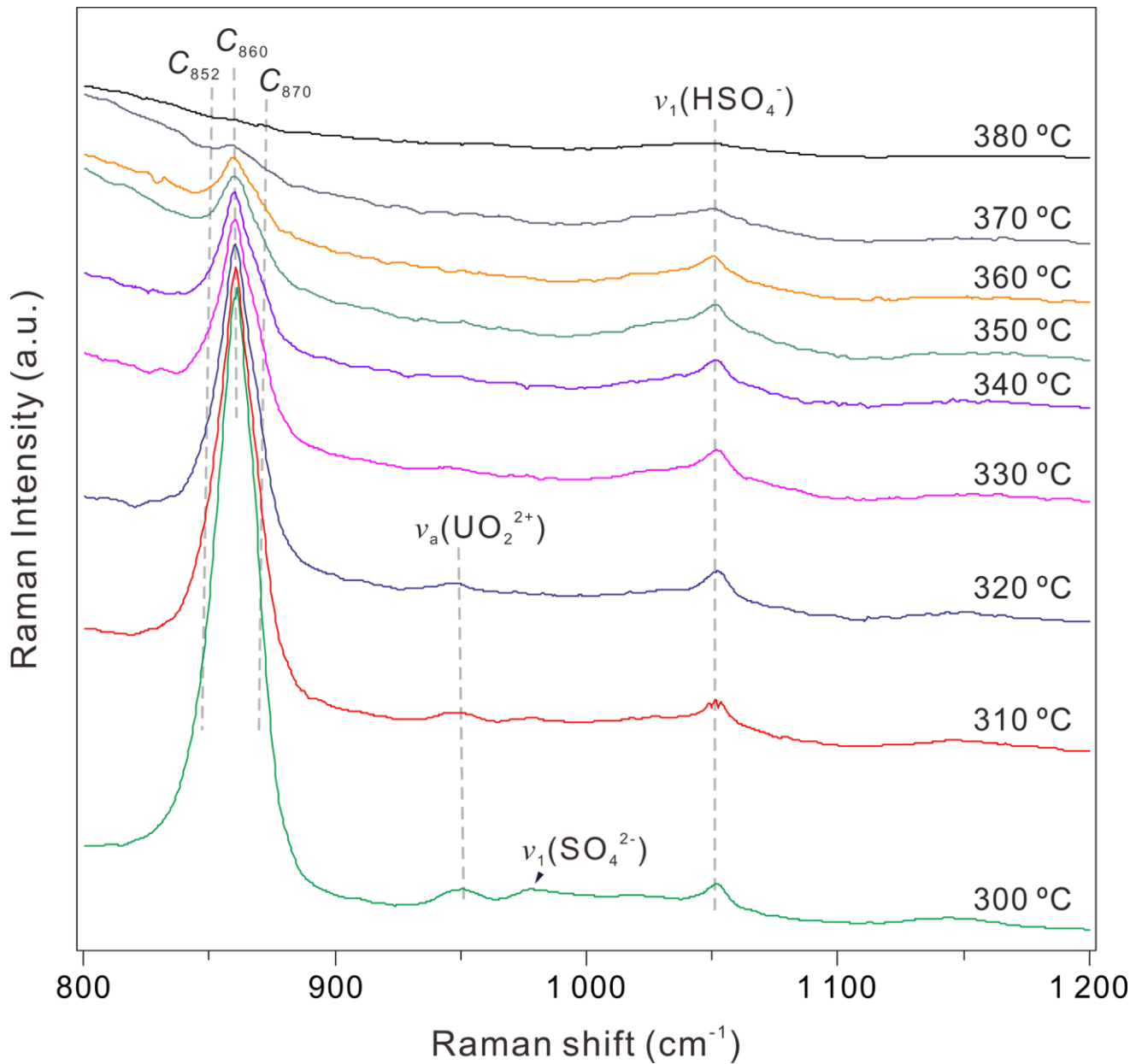


Fig. 6. Variation of peak area ratios between $\nu_1(\text{UO}_2^{2+})$ and $\nu_s(\text{H}_2\text{O})$ bands ($A_{\text{Uranyl}}/A_{\text{water}}$) of U_{rich} (squares) and U_{poor} (circles) liquids as a function of temperature in 0.54 mol/kg UO_2SO_4 solution.

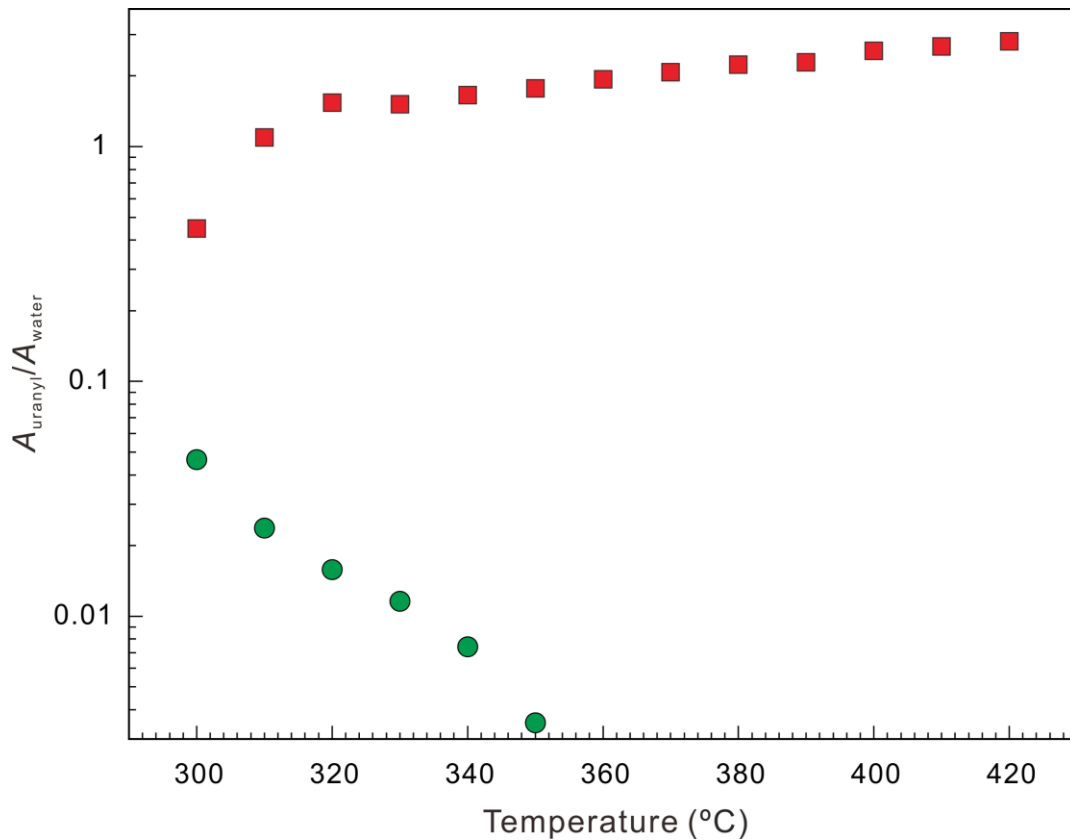


Fig. 7. Spectra of $\nu_1(\text{SO}_4^{2-})$ bands normalized by $\nu_1(\text{UO}_2^{2+})$ -intensity for immiscible liquids in 0.54 mol/kg UO_2SO_4 . U_{rich} liquids at 350 °C (a) and 300 °C (b); and U_{poor} liquids at 350 °C (c) and 300 °C (d).

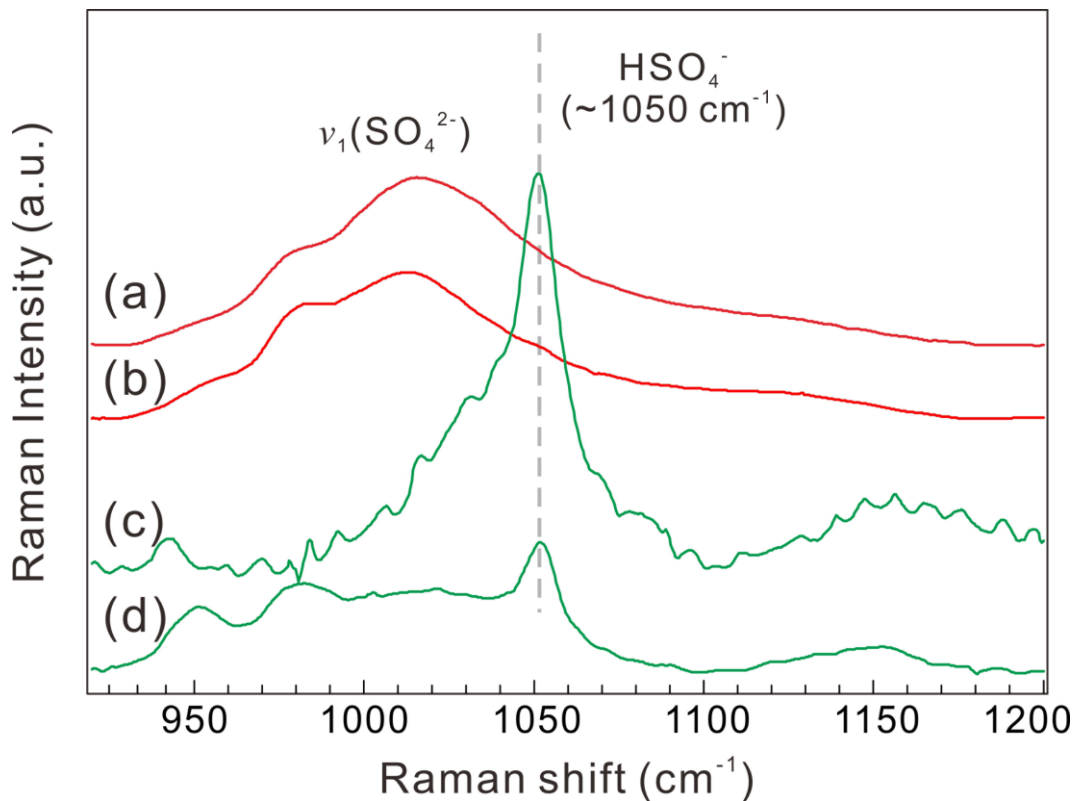


Table 1. Observed temperatures for the occurrence of liquid-liquid immiscibility for aqueous UO_2SO_4 solutions at saturated vapor pressures.

UO_2SO_4 (mol/kg)	Temperature ($^{\circ}\text{C}$)	Standard Deviation ($^{\circ}\text{C}$)
0.18	300	0.5
0.36	287	0.2
0.54	285.8	0.5
0.71	286	0.1
0.88	286.2	0.1
1.04	287.2	0.2